Computational Mathematics and Mathematical Physics, Vol. 40, No. 11, 2000, pp. 1617–1637.
Translated from Zhurnal Vychislitel'noi Matematiki i Matematicheskoi Fiziki, Vol. 40, No. 11, 2000, pp. 1685–1705.

Barrier Method for Quasi-Isometric Grid Generation

V. A. Garanzha

Computing Center, Russian Academy of Sciences, ul. Vavilova 40, Moscow, 117967 Russia

Received January 18, 2000; in final form, April 18, 2000

Abstract—A gridgeneration method based on the minimization of a barrier functional with a feasible set consisting of quasi-isometric grids is presented. The procedure for minimizing the deviation from isometry for a grid of given connectivity and for given boundary grid points makes it possible to contract the feasible set into a small neighborhood of the optimal solution. Since the functional is defined in terms of metrics in both physical and logical coordinates, the adaptation problem can be analyzed within the framework of quasi-isometric grids. A reliable and efficient technique for constructing a feasible solution is proposed, based on the penalty formulation and continuation technique. Numerical experiments demonstrate the high quality of the generated grids.

1. INTRODUCTION

The class of the most reliable gridgeneration methods is based on the variational principle. In particular, this concerns methods involving quasi-conformal mappings [1, 2] and harmonic mappings [3–6]. In those studies, grids were generated by minimizing a discrete counterpart of the Dirichlet functional and its generalizations.

In the general case, the problem of variational grid generation is posed so that a certain measure of quality is maximized under the condition that all grid cells are nondegenerate. In other words, it is a conditional minimization problem.

Suppose that a desired grid in the n-dimensional space $\{x_1, \ldots, x_n\}$ can be represented as a vector:

$$\mathbf{R} = \begin{pmatrix} \mathbf{X}^1 \\ \cdots \\ \mathbf{X}^n \end{pmatrix}, \quad \mathbf{X}^i \in \mathbb{R}^{N_v},$$

where $\mathbf{X}^i$ is the vector of all x_i-components of grid points, and N_v is the total number of grid points. Let us seek $\mathbf{R}$ as a result of minimization of a functional $\mathcal{J}^h(\mathbf{R})$ defined on an open feasible set $\mathcal{F}$ of nondegenerate grids of prescribed connectivity with prescribed boundary points. Consider only the grid functionals that are at least twice differentiable, positive, and bounded functions of $\mathbf{R}$ on any connected subset of $\mathcal{F}$ under the condition

$$\lim_{\mathbf{R} \in \mathcal{F},\ \operatorname{dist}(\mathbf{R}, \partial\mathcal{F}) \to 0} \mathcal{J}^h(\mathbf{R}) = +\infty. \tag{1.1}$$

The existence of this barrier (a barrier of the first kind) ensures that the functional has at least one stationary point inside the feasible set. It was shown in [6, 7] that some discrete approximations of the generalized Dirichlet functional have similar barriers at the boundaries of the set of grids consisting of convex quadrilaterals.

The gradient of a barrier functional should possess barrier property as well:

$$\lim_{\mathbf{R} \in \mathcal{F},\ \operatorname{dist}(\mathbf{R}, \partial\mathcal{F}) \to 0} \left\| \nabla \mathcal{J}^h(\mathbf{R}) \right\| = +\infty, \tag{1.2}$$

where $\|\cdot\|$ denotes, for example, the Euclidean norm in $\mathbb{R}^{nN_v}$. The existence of this barrier of the second kind ensures that there exists a constant c such that $\operatorname{dist}(\mathbf{R}_s, \partial\mathcal{F}) \geq c > 0$, where $\mathbf{R}_s$ is a stationary point of $\mathcal{J}^h(\mathbf{R})$. The simple one-dimensional example involving the function

$$f(x) = [2 + \sin(1/x)]/x, \quad \mathcal{F} = \{x, x > 0\},$$

where stationary points are located in an arbitrarily small neighborhood of the boundary of the feasible set, illustrates the importance of this property for nonconvex functionals.

Similar problems arise in the mechanics of hyperelastic solids, where nondegenerate mappings are to be constructed. This motivated the formulation of the principle of extremal states [8–10], which appears to be equivalent to the requirement for the existence of a barrier of the second kind. Moreover, it was shown in [9] that the principle of extremal states formulated for continua so as to ensure that a mapping is nondegenerate is incompatible with the convexity of the functional for which the desired mapping is a stationary point. Consequently, convexity cannot be expected in the case of a grid barrier functional, which was numerically confirmed in [11]. The proof of (1.2) for the functionals considered in this paper is a difficult task that has not been accomplished to this day.

Practical generation of admissible grids for barrier functionals can be based on replacing a barrier with a penalty function. Accordingly, $\mathcal{I}^h(\mathbf{R})$ is replaced with a regularized functional $\mathcal{I}^h_\varepsilon(\mathbf{R})$ having the following properties:

$$\lim_{\mathbf{R} \in \mathcal{F},\, \varepsilon \to 0} \left| \mathcal{I}^h(\mathbf{R}) - \mathcal{I}^h_\varepsilon(\mathbf{R}) \right| = 0, \qquad \lim_{\mathbf{R} \notin \mathcal{F},\, \varepsilon \to 0} \mathcal{I}^h_\varepsilon(\mathbf{R}) = +\infty, \tag{1.3}$$

$$\lim_{\mathbf{R} \notin \mathcal{F},\, \varepsilon \to 0} \left\| \nabla \mathcal{I}^h_\varepsilon(\mathbf{R}) \right\| = +\infty. \tag{1.4}$$

Here, $\mathcal{I}^h_\varepsilon(\mathbf{R})$ is an at least twice differentiable function defined on the entire space. One approach of this kind was proposed in [11]. As a rule, property (1.3) is relatively easy to prove, whereas property (1.4), which guarantees that the limit stationary points of the penalty functional belong to the feasible set, is difficult to prove and has been proved only in some special cases.

Recently, it became common practice that unstructured grids are "smoothed" by applying the variational method element by element. This method relies on a functional that maximizes the quality of local mapping for each individual cell and gives the sum of contributions of all cells based on the conventional assembling procedure of the finite element method. As applied to structured grids, this method is equivalent to discrete domain-mapping methods. It can also be applied to block-structured grids. In this paper, the functional is derived for a structured grid and then is extended to unstructured grids.

The functional $\mathcal{I}^h(\mathbf{R})$ can be constructed by invoking a variety of quality measures (see [5, 12–15]). When using the quality measure t, which is "dimensionless" in the sense that $0 \le t \le 1$, one may consider a parameterized feasible set $\mathcal{F}(t)$ of grids in which every cell has a quality measure higher than the threshold value of t. In this case, $\mathcal{F}(0)$ denotes the set of nondegenerate grids, and $\mathcal{F}(1)$ denotes a grid consisting of "perfect" cells. As a rule, barriers are constructed on $\partial\mathcal{F}(0)$. The basic idea of this study is that the barrier should be constructed on $\partial\mathcal{F}(t)$ and "contracted" so as to obtain a sequence of nested feasible sets and, finally, a maximal value of the quality measure, $t = t_{\max}$.

If it can be shown that

$$\mathcal{F}(t_1) \subset \mathcal{F}(t_2), \quad t_1 > t_2, \text{ and } \mathcal{F}(t) = \varnothing, \quad t > 1,$$

then one may expect that, for a given grid connectivity and fixed boundary points, there exists $0 < t = t_{\max} \le 1$ such that

$$\lim_{t \to t_{\max},\, t \le t_{\max}} \operatorname{diam}(\mathcal{F}(t)) = 0,$$

provided that $\mathcal{F}(0)$ is simply connected. The relationship between various barriers thus obtained is illustrated in Fig. 1. This is quite an optimistic scenario, because one may also expect that the measure, rather than diameter, of the feasible set should tend to zero and, in particular, that the feasible set for $\mathcal{F}(t)$ $t > t_0 \ge 0$ is the union of nonintersecting simply connected domains for which the diameters of limit feasible sets tend to zero. It should be noted that the global extremum search within a single simply connected set does not make sense in the context of grid generation, because one principal requirement for a grid generation method is that the result must be continuously dependent on input data. When a nonunique result is obtained, this condition is violated, and any grid in the neighborhood of the set of quasi-solutions can be taken as a solution. This sets natural limits on the contraction of the feasible set. It is a well-known fact that barrier grid functionals have multiple stationary points [11], but the conditions that guarantee uniqueness are not known.

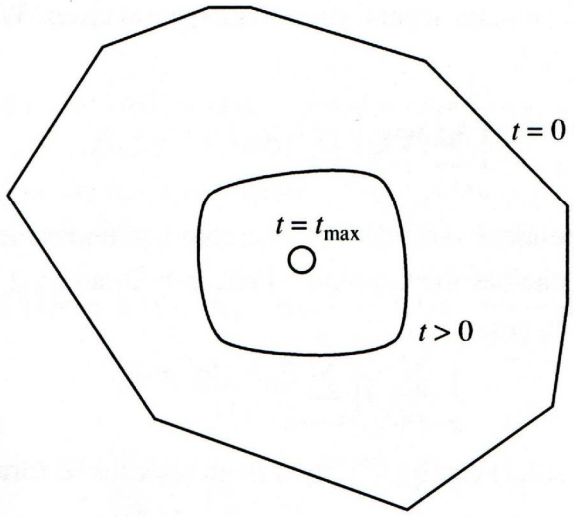

Fig. 1.

Thus, the barrier grid generation method must include the following components: (a) a variational principle, (b) a procedure for contracting a feasible set, (c) a penalty formulation and technique for constructing a feasible solution, and (d) an efficient minimization method.

In this paper, items (a)–(c) are addressed. The minimization method is close to that employed in [11], but is more complicated, and its description should be presented in a separate publication.

Since construction of mappings is simply an auxiliary task rather than the ultimate goal in the context of the present analysis, validation of functionals, solvability, and regularity of solutions in the continuous case are not addressed here.

2. VARIATIONAL PRINCIPLE

Let us seek the vector function

$$\mathbf{r} = \mathbf{r}(\xi_1, \ldots, \xi_n), \quad \mathbf{r} = (x_1, \ldots, x_n)^{\mathrm{T}} \tag{2.1}$$

that defines a one-to-one mapping of a domain $\mathcal{D}$ of regular shape (e.g., the unit cube) in a logical coordinate system $\{\xi_1, \ldots, \xi_n\}$ to a physical domain Ω. In what follows, mappings of other regularly shaped domains (in particular, tetrahedra for $n = 3$) are also considered.

Henceforth, the following notation is employed:

$$\mathbf{g}_i = \partial\mathbf{r}/\partial\xi_i, \quad S = (\mathbf{g}_1, \ldots, \mathbf{g}_n), \quad \mathrm{adj}S = S^{-1}\det S, \quad (\mathbf{g}^1, \ldots, \mathbf{g}^n) = \mathrm{adj}S^{\mathrm{T}},$$

where $\mathbf{g}_i$ denotes covariant basis vectors, and S is the Jacobian matrix. The determinant and trace of a matrix are denoted by det and tr, respectively.

Following the theory of harmonic mappings [16], let us begin the analysis by seeking the mapping in (2.1) as the inverse of a harmonic mapping or as a solution to the following problem:

$$\operatorname*{argmin}_{\mathbf{r}(\xi)} \int_{\mathcal{D}} \frac{\mathrm{tr}(H^{\mathrm{T}}H\,\mathrm{adj}S G^{-1}\mathrm{adj}S^{\mathrm{T}})}{(\det G)^{-1/2}\det S} d\xi, \tag{2.2}$$

subject to the condition

$$\det S > 0.$$

A one-to-one mapping between $\partial\mathcal{D}$ and $\partial\Omega$ is assumed to be prescribed.

Here, $G = G^{\mathrm{T}} > 0$, $G = G(\mathbf{r})$ is a prescribed metric in physical coordinates, $H = H(\xi)$ and $H^{\mathrm{T}}H > 0$ is the "accompanying" metric defined in the logical space.

The general formulation (2.2) entails several important special cases. When $H = I$, one has the generalized Dirichlet functional [14]

$$\int_{\Omega} \sum_{i=1}^{n} (\nabla \xi_i)^{\mathrm{T}} G^{-1} (\det G)^{1/2} \nabla \xi_i dx.$$

Here, both dependent and independent variables are interchanged under the assumption that $\det S > 0$.

In another limit case, $G = I$, one has the Godunov–Prokopov functional [17]

$$\int_{\mathcal{D}} \sum_{i,j=1}^{n} \frac{1}{J} \left(\sum_{k=1}^{n} h_{ki} h_{kj} \right) \mathbf{g}^{i^{\mathrm{T}}} \mathbf{g}^{j} d\xi.$$

In the two-dimensional case, (2.2) can be rewritten in an alternative form. Using the identity

$$\operatorname{tr}(H^{\mathrm{T}} H \operatorname{adj} S G^{-1} \operatorname{adj} S^{\mathrm{T}}) = \operatorname{tr}(\operatorname{adj} G^{-1} S \operatorname{adj}(H^{\mathrm{T}} H) S^{\mathrm{T}}),$$

which is valid only for 2-by-2 matrices, we obtain

$$\frac{\operatorname{tr}(H^{\mathrm{T}} H \operatorname{adj} S G^{-1} \operatorname{adj} S^{\mathrm{T}})}{(\det G)^{-1/2} \det S} = \frac{(\det H)^2 \operatorname{tr}(H^{-\mathrm{T}} S^{\mathrm{T}} G S H^{-1})}{(\det G)^{1/2} \det S}.$$

Introducing

$$A = H^{-\mathrm{T}} S^{\mathrm{T}}, \tag{2.3}$$

we obtain

$$\frac{\operatorname{tr}(H^{\mathrm{T}} H \operatorname{adj} S G^{-1} \operatorname{adj} S^{\mathrm{T}})}{(\det G)^{-1/2} \det S} = \frac{\det H \operatorname{tr}(G A^{\mathrm{T}} A)}{(\det G)^{1/2} \det A} = f(A),$$

and functional (2.2) can be rewritten as

$$\int_{\mathcal{D}} f(A) d\xi. \tag{2.4}$$

As the next step, an extension of (2.4) to the n-dimensional case is considered as the dimensionless ratio of matrix invariants [18]:

$$f(A) = \det H \left[\frac{1}{n} \operatorname{tr}(G A^{\mathrm{T}} A) \right]^{n/2} [\det A (\det G)^{1/2}]^{-1} = \frac{\det H}{\det A} \varphi_c, \quad \varphi_c = \left[\frac{1}{n} \operatorname{tr}(G A^{\mathrm{T}} A) \right]^{n/2} (\det G)^{-1/2}. \tag{2.5}$$

It is obvious that $f(A)$ is invariant with respect to scaling of A. Therefore, we can add to (2.5) a term that controls the value of $\det A$:

$$f(A) = \frac{\det H}{\det A} \varphi(A), \quad \varphi(A) = (1 - \omega_u) \varphi_c + \omega_u \varphi_u, \quad \varphi_u = \frac{1}{2} \left(\frac{\bar{v}}{(\det G)^{1/2}} + \frac{(\det G)^{1/2}}{\bar{v}} (\det A)^2 \right), \tag{2.6}$$

where

$$\bar{v} = \int_{\mathcal{D}} (\det G)^{1/2} \det S d\xi \left(\int_{\mathcal{D}} \det H d\xi \right)^{-1}, \quad 0 < \omega_u < 1.$$

To analyze the properties of the function $f(A)$ defined by (2.6), consider the auxiliary minimization problem

$$\operatorname*{argmin}_{A} f(A). \tag{2.7}$$

Omitting calculations, we can write out the solution to the Euler–Lagrange equations corresponding to this

functional with $\det A > 0$:

$$AGA^{\mathrm{T}} = \frac{1}{n}\mathrm{tr}(GA^{\mathrm{T}}A)I, \quad \det A = \frac{\overline{\nu}}{(\det G)^{1/2}}, \tag{2.8}$$

where $\varphi(A) = \det A$ on the solution, so that $f(A) = \det H$.

By the definition of A, (2.8) is equivalent to

$$S^{\mathrm{T}}GS = \overline{\nu}^{2/n}H^{\mathrm{T}}H, \quad \det S = \det H\frac{\overline{\nu}}{(\det G)^{1/2}},$$

or

$$\sum_{k,p=1}^{n}\frac{\partial x_i}{\partial \xi_k}g_{kp}\frac{\partial x_j}{\partial \xi_p} = \overline{\nu}^{2/n}\sum_{k=1}^{n}h_{ki}h_{kj}. \tag{2.9}$$

Here, g_{kp} denotes the covariant components of the metric G, and $\Sigma_{k=1}^{n}h_{ki}h_{kj}$ is the ijth component of the metric $H^{\mathrm{T}}H$. Thus, (2.9) provides a rule for transforming the covariant components of a tensor. This means that both G and $H^{\mathrm{T}}H$ represent the same tensor of rank 2 written in different coordinates up to a constant factor. This also implies that the functional in (2.6) can be interpreted as a measure of deviation of one tensor from the other. The fact that a harmonic functional is a measure of tensor deviation up to an arbitrary factor in the two-dimensional case was established by Godunov [19]. However, the addition of an "incompressibility" term can be used to control the constant at any point. Incompressible mapping is generally construed as a locally volume-preserving one, but we can extend it to the case of $\overline{\nu} \neq 1$, which corresponds to global scaling.

As a result, (2.1) is an isometric (i.e., both conformal and incompressible) mapping in the ideal case, and

$$(dl_r)^2 = \overline{\nu}^{2/n}(dl_\xi)^2,$$

where dl_r and dl_ξ are the length differentials in Ω and $\mathcal{D}$, respectively, calculated in the respective metrics:

$$|dl_\xi| = |(d\xi_1, \ldots, d\xi_n)H^{\mathrm{T}}|, \quad |dl_r| = |d\mathbf{r}^{\mathrm{T}}Gd\mathbf{r}|^{1/2}, \quad d\mathbf{r}^{\mathrm{T}} = (d\xi_1, \ldots, d\xi_n)S^{\mathrm{T}}.$$

It is obvious that the perfectly isometric minimum can be attained in certain special cases only.

The problem of constructing quasi-isometric mappings, formulated by Godunov [19], is stated in the present notation as follows. Find a mapping $\mathbf{r}(\xi_1, \ldots, \xi_n)$ such that

$$\gamma^2\overline{\nu}^{2/n}(dl_\xi)^2 < (dl_r)^2 < \Gamma^2\overline{\nu}^{2/n}(dl_\xi)^2, \quad \Gamma \geq \gamma > 0, \tag{2.10}$$

and the ratio Γ/γ (i.e., the isometric condition number) is minimized over all mappings satisfying given boundary conditions. Relation (2.10) can be written in the matrix form as

$$\gamma^2\overline{\nu}^{2/n}I < AGA^{\mathrm{T}} < \Gamma^2\overline{\nu}^{2/n}I, \text{ or } \gamma^2\overline{\nu}^{2/n}H^{\mathrm{T}}H < S^{\mathrm{T}}GS < \Gamma^2\overline{\nu}^{2/n}H^{\mathrm{T}}H,$$

where $\mathbf{r}$ and ξ are related through (2.1).

It is not quite obvious whether the minimum of the functional defined by (2.4) and (2.6) is a quasi-isometric mapping. For this reason, let us consider another function $f(A)$ whose feasible set consists of mappings satisfying (2.10). In particular, the auxiliary minimization problem

$$\operatorname*{argmin}_A f(A), \quad f(A) = (1-t)\det H\frac{\varphi(A)}{\det A - t\varphi(A)},$$

where $0 < t \leq 1$, is also solved by (2.8), provided that $\det A - t\varphi(A) > 0$. Similar transformations of the starting problem, which preserve stationary points, are widely used in nonlinear programming methods [20].

Thus, the minimization problem

$$\operatorname*{argmin}_{\mathbf{r}(\xi)}(1-t)\int_{\mathcal{D}}\det H\frac{\varphi(A)}{\det A - t\varphi(A)}d\xi, \quad A = (\mathbf{a}_1, \ldots, \mathbf{a}_n), \quad \mathbf{a}_i = (H^{\mathrm{T}})^{-1}\nabla_\xi x_i \tag{2.11}$$

is formulated under the constraint

$$\det A - t\varphi(A) > 0. \tag{2.12}$$

Here, ∇_ξ is the gradient operator in the logical coordinates; i.e., $\nabla_\xi x_i = (\partial x_i/\partial\xi_1, \ldots, \partial x_i/\partial\xi_n)^T$, and $\varphi(A)$ is defined by (2.6).

One may also consider a modified formulation of (2.11):

$$\operatorname*{argmin}_{\mathbf{r}(\xi)}(1-t)\int_{\mathcal{D}}\frac{\psi(H)\varphi(A)}{\det A - t\psi(H)\varphi(A)}d\xi, \tag{2.13}$$

where the form of $\psi(H)$ depends on the specific problem in question. The functional in (2.13) is used below to construct grids that are orthogonal to domain boundaries.

2.1. Characterization of the Feasible Set

Let us show that the feasible set $\mathcal{F}(t)$ defined by (2.12) consists of quasi-isometric mappings. Indeed, (2.12) implies that

$$\frac{\varphi_c}{\det A} < c_1 = \frac{1-\omega_u t}{(1-\omega_u)t}, \quad \frac{\varphi_u}{\det A} < c_2 = \frac{1-(1-\omega_u)t}{\omega_u t}.$$

Introducing $V = AGA^T$, we obtain

$$\left(\frac{1}{n}\operatorname{tr}V\right)^{n/2}(\det V)^{-1/2} < c_1, \quad \frac{\bar{v}}{(\det V)^{1/2}} + \frac{(\det V)^{1/2}}{\bar{v}} < 2c_2$$

or

$$(\beta(V))^{n/2} < c_1, \quad c_2 - \sqrt{c_2^2-1} < \frac{(\det V)^{1/2}}{\bar{v}} < c_2 + \sqrt{c_2^2-1},$$

where

$$\beta(V) = \frac{1}{n}\operatorname{tr}V(\det V)^{-1/n}$$

is the spherical measure, or Kaporin's condition number, of the matrix V. With the use of Kaporin's inequality [21] relating $\beta(V)$ to the spectral condition number $\operatorname{cond}(V)$,

$$\operatorname{cond}(V) \le \left[\sqrt{(\beta(V))^n} + \sqrt{(\beta(V))^n - 1}\right]^2,$$

which is valid for any symmetric, positive definite matrix V, we obtain

$$\left(c_1 - \sqrt{c_1^2-1}\right)^2 < \frac{\lambda_i(V)}{\lambda_j(V)} < \left(c_1 + \sqrt{c_1^2-1}\right)^2,$$

where $\lambda_i(V)$, $\lambda_j(V)$ is any pair of eigenvalues of V. Thus, the final estimate for (2.10) is given by

$$\gamma = \left(c_2 - \sqrt{c_2^2-1}\right)^{1/n}\left(c_1 - \sqrt{c_1^2-1}\right)^{(n-1)/n}, \quad \Gamma = \left(c_2 + \sqrt{c_2^2-1}\right)^{1/n}\left(c_1 + \sqrt{c_1^2-1}\right)^{(n-1)/n}, \tag{2.14}$$

which implies that γ is a monotone increasing function of t, and Γ is a monotone decreasing function of t. The estimates in (2.14) are rough and are attained by isometric mappings only.

This problem can be circumvented by using functional (2.4) with

$$f(A) = \det H\left((1-\omega_u)\frac{\varphi_c}{\det A - t\varphi_c} + \omega_u\frac{\varphi_u}{\det A - t\varphi_u}\right).$$

In this case, the feasible set $\mathcal{F}(t)$ is defined as

$$\mathcal{F}(t) = \mathcal{F}_c(t) \cap \mathcal{F}_u(t),$$

where $\mathcal{F}_c(t)$ consists of quasi-conformal mappings, $\mathcal{F}_u(t)$ consists of quasi-incompressible mappings, and

$$\frac{\Gamma}{\gamma} = \left(\frac{1}{t} + \sqrt{\frac{1}{t^2}-1}\right)^2.$$

However, it is difficult to handle two different barriers simultaneously in dealing with a nonlinear and nonconvex problem. For this reason, the present analysis is restricted to functional (2.11).

In [22], it was shown that quasi-isometric functionals, indicated above are elliptic in the feasible domain if $t \geq 0$.

2.2. *Penalty Formulation*

In view of the practical success of the technique proposed in [1], it is proposed here that problem (2.11) subject to constraint (2.12) be replaced by problem

$$\mathbf{r}(\xi) = \lim_{\varepsilon \to \varepsilon_l, \varepsilon \geq \varepsilon_l} \operatorname{argmin}_{\mathbf{r}(\xi)} \mathcal{J}_\varepsilon, \tag{2.15}$$

where

$$\mathcal{J}_\varepsilon = \int_{\mathcal{D}} \det H \frac{\varphi(A)}{\chi_\varepsilon[\det A - t\varphi(A)]} d\xi \tag{2.16}$$

and

$$\chi_\varepsilon(q) = \frac{q}{2} + \frac{1}{2}\sqrt{\varepsilon^2 + q^2}, \quad q = \det A - t\varphi(A), \tag{2.17}$$

and $\varepsilon_l > 0$ is sufficiently small. For brevity, the argument q in $\chi_\varepsilon(q)$ is omitted where possible, and the symbols $\chi'_\varepsilon = \partial\chi_\varepsilon/\partial q$ and $\chi''_\varepsilon = \partial^2\chi_\varepsilon/\partial^2 q$ are used. The function χ_ε has the following properties:

$$\chi_\varepsilon \approx q, \quad q \longrightarrow +\infty; \quad \chi_\varepsilon \approx \frac{1}{4}\frac{\varepsilon^2}{|q|}, \quad q \longrightarrow -\infty, \quad \left|\frac{\chi'_\varepsilon q}{\chi_\varepsilon}\right| \leq 1, \quad \chi'^2_\varepsilon - \frac{1}{2}\chi_\varepsilon\chi''_\varepsilon \geq 0. \tag{2.18}$$

It is obvious that a set of such functions can be constructed, but the remarkable properties (2.18) make the hyperbolic penalty function proposed by Kaporin a very good regularizer for (2.11), (2.12).

A similar penalty function was proposed in [23] for smoothing triangular grids, based on an analogy with a system of springs characterized by nonlinear elasticity:

$$\tilde{\chi}_\varepsilon(q) = \begin{cases} q, & q > \varepsilon, \\ \varepsilon^2/(2\varepsilon - q), & q \leq \varepsilon. \end{cases}$$

However, the variational principle was not invoked in [23]. The function χ_ε is obviously more suitable for a variational method, because it is infinitely differentiable and $1/\chi_\varepsilon$ is a convex function, which is not the case with $1/\tilde{\chi}_\varepsilon$.

3. BARRIER APPROXIMATIONS OF THE FUNCTIONAL

Suppose that a valid grid connectivity is defined by N_c cells. In a cell with index c, denote by $\mathbf{R}_c$ the vector of all of its vertices:

$$\mathbf{R}_c = \begin{pmatrix} \mathbf{X}_c^1 \\ \dots \\ \mathbf{X}_c^n \end{pmatrix}, \quad \mathbf{X}_c^i \in \mathbb{R}^{N_{cv}},$$

where N_{cv} is the number of vertices in the cell.

When a cell $\mathcal{D}_c$ is specified by an ordered set of N_{cv} of integer numbers $v_1(c), \dots, v_{N_{cv}}(c)$ indicating the cell's vertices in the complete list of vertices, it holds that

$$\mathbf{X}_c^i = \mathcal{R}_c \mathbf{X}^i,$$

where the restriction matrix $R_c \in \mathbb{R}^{N_{cv} \times N_v}$ is defined as

$$\mathcal{R}_c = \{r_{ij}\}, \quad r_{ij} = \begin{cases} 1, & j = v_i(c) \\ 0, & j \neq v_i(c). \end{cases}$$

Using this notation, we can formulate a discrete counterpart of problem (2.15): find a vector $\mathbf{R}$ that solves the minimization problem

$$\mathbf{R} = \lim_{\varepsilon \to \varepsilon_l,\, \varepsilon \geq \varepsilon_l} \operatorname{argmin}_{\mathbf{R}} \mathcal{J}_\varepsilon^h(\mathbf{R}, t), \quad \mathcal{J}_\varepsilon^h(\mathbf{R}, t) = \sum_{c=1}^{N_c} \sum_{q(c)=1}^{N_q} f_\varepsilon(A)|_{q(c)} \sigma_{q(c)}, \quad f_\varepsilon(A) = \det H \frac{\varphi(A)}{\chi_\varepsilon[\det A + t\varphi(A)]}, \tag{3.1}$$

$$\varphi(A) = (1 - \omega_u)\varphi_c + \omega_u \varphi_u, \quad \mathbf{a}_i|_{q(c)} = (H_{q(c)}^{\mathrm{T}})^{-1} Q_{q(c)} \mathbf{X}_c^i, \quad \mathbf{X}_c^i = \mathcal{R}_c \mathbf{X}^i,$$

where $q(c)$ is the index of the qth quadrature point in the approximation of the integral over the cell $\mathcal{D}_c$, and each of the N_q matrices $Q_{q(c)}$ actually describes the approximation of functional (2.16) on the corresponding element. The present analysis is restricted to quadratures with positive weighting factors:

$$\sum_{q(c)=1}^{N_q} \sigma_{q(c)} = 1, \quad \sigma_{q(c)} > 0.$$

Suppose also that G is constant within each cell, e.g.,

$$G|_c = \int_{\mathcal{D}_c} G(\mathbf{r}(\xi_1, \ldots, \xi_n)) d\xi \left(\int_{\mathcal{D}} d\xi \right)^{-1},$$

although G can be averaged in the physical coordinates as well. An optimal approach would require additional analysis.

The feasible set $\mathcal{F}^h(t)$ is defined by $N_c N_q$ nonlinear inequalities

$$\det A - t\varphi(A)|_{q(c)} > 0. \tag{3.2}$$

Accordingly, the grid quasi-isometry conditions are written as $N_c N_q$ inequalities

$$\bar{v}^{2/n} \gamma^2 I \leq A G A^{\mathrm{T}}|_{q(c)} \leq \bar{v}^{2/n} \Gamma^2 I,$$

where the volume factor $\bar{v}$ is expressed as

$$\bar{v} = \sum_{c=1}^{N_c} \int_{\mathcal{D}_c} (\det G)^{1/2} \det S d\xi \left(\sum_{c=1}^{N_c} \int_{\mathcal{D}_c} \det H d\xi \right)^{-1}.$$

Henceforth, the ratio Γ/γ is referred to as the grid condition number. Since the values of γ and Γ are equal for all grid cells, the minimization problem for the isometric condition number can be subsumed under the class of global minimization problems.

To take into account boundary conditions, $\mathbf{R}$ is sought in the form

$$\mathbf{X}^i = (I - M)\mathbf{X}_b^i + M\mathbf{X}_{in}^i, \tag{3.3}$$

where $M \in \mathbb{R}^{N_v \times N_v}$ is a diagonal matrix with entries m_{ij} such that $m_{ii} = 1$ if the ith grid point is an interior one; $m_{ii} = 0$ if the ith grid point is a fixed boundary one; and $\mathbf{R}_b$ and $\mathbf{R}_{in}$ denote a prescribed vector satisfying boundary conditions and an unknown vector, respectively.

Lexicographic numbering is used locally within each grid cell as illustrated by Fig. 2. For convenience, triple indexing is also used in the three-dimensional case.

An analysis of discrete problem (3.1) shows that all integrals and their discrete approximations can be written in terms of local coordinates for each element. In other words, the fact that the grid is structured is never used in explicit form, so that the same functional can be employed in the case of an unstructured grid as well.

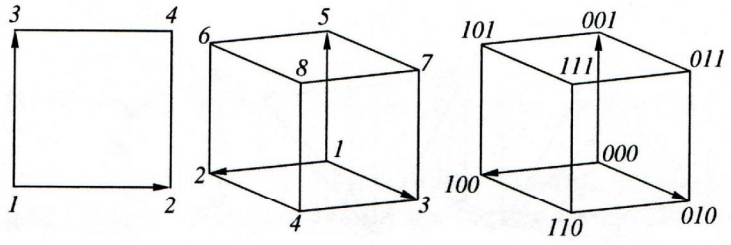

Fig. 2.

3.1. Barrier for an Invertible Bilinear Mapping

A bilinear mapping is invertible if and only if the quadrilateral cell is convex [24]. Under this condition, the coordinate vector $\mathbf{r}$ is written in local coordinates as follows:

$$\mathbf{r}(\xi_1, \xi_2) = (1-\xi_1)(1-\xi_2)\mathbf{r}(0,0) + (1-\xi_1)\xi_2\mathbf{r}(0,1) + \xi_1(1-\xi_2)\mathbf{r}(1,0) + \xi_1\xi_2\mathbf{r}(1,1),$$

and the vectors $\mathbf{a}_1$ and $\mathbf{a}_2$ have the form

$$\mathbf{a}_i = (H^{\mathrm{T}})^{-1} W^{\mathrm{T}}(\xi_1, \xi_2)\mathbf{X}_c^i, \quad W(\xi_1, \xi_2) = (\mathbf{w}_1, \mathbf{w}_2) = \begin{pmatrix} \xi_2 - 1 & 1-\xi_2 & -\xi_2 & \xi_2 \\ \xi_1 - 1 & -\xi_1 & (1-\xi_1) & \xi_1 \end{pmatrix}^{\mathrm{T}}.$$

Using the trapezoid quadrature formula, one obtains

$$Q_{2k+j+1} = W(j,k), \quad j,k \in \{0,1\}, \quad N_q = 4, \quad \sigma_i = 1/4. \tag{3.4}$$

Accordingly, the functional has a barrier on the boundary of the set of grids with convex cells when $t = 0$ [6].

3.2. Barrier Approximations for Hexahedral Cells

In the three-dimensional case, the basic restriction in constructing the functional is that the resulting grids be admissible for the approximation scheme used for solving problems on them. To comply with this requirement, one may use the same approach in approximating the grid functional and the equations to be solved on the grids. Here, only schemes that calculate a trilinear cell volume exactly are considered, i.e., satisfy the patch test in the sense of [24]. Construction of barrier approximations for harmonic functional (2.2) is a difficult task in the three-dimensional case [25, 26], but the difficulties are eliminated by using functional (2.11). Nonetheless, only approaches that apply to the harmonic functional as well are considered here.

Denoting the eight vertices of a cell by $\mathbf{r}^{000}$, $\mathbf{r}^{100}$, $\mathbf{r}^{010}$, $\mathbf{r}^{110}$, $\mathbf{r}^{001}$, $\mathbf{r}^{101}$, $\mathbf{r}^{011}$, and $\mathbf{r}^{111}$, we can write the trilinear mapping of the unit cube to a straight-edged hexahedron as

$$\begin{aligned}\mathbf{r}(\xi_1, \xi_2, \xi_3) &= (1-\xi_1)(1-\xi_2)(1-\xi_3)\mathbf{r}^{000} + \xi_1(1-\xi_2)(1-\xi_3)\mathbf{r}^{100} + (1-\xi_1)\xi_2(1-\xi_3)\mathbf{r}^{010} \\ &+ (1-\xi_1)(1-\xi_2)\xi_3\mathbf{r}^{001} + \xi_1\xi_2(1-\xi_3)\mathbf{r}^{110} + \xi_1(1-\xi_2)\xi_3\mathbf{r}^{101} + (1-\xi_1)\xi_2\xi_3\mathbf{r}^{011} + \xi_1\xi_2\xi_3\mathbf{r}^{111},\end{aligned} \tag{3.5}$$

where

$$\mathbf{r}^{ijk} = \mathbf{r}(i,j,k), \quad i,j,k \in \{0,1\},$$

as illustrated by Fig. 2.

Using once again the auxiliary vectors $w_i(\xi_1, \xi_2, \xi_3)$ $(i = 1, 2, 3)$ such that

$$\mathbf{a}_i = H^{-\mathrm{T}} \begin{pmatrix} \mathbf{w}_1^{\mathrm{T}}\mathbf{X}_c^i \\ \mathbf{w}_2^{\mathrm{T}}\mathbf{X}_c^i \\ \mathbf{w}_3^{\mathrm{T}}\mathbf{X}_c^i \end{pmatrix},$$

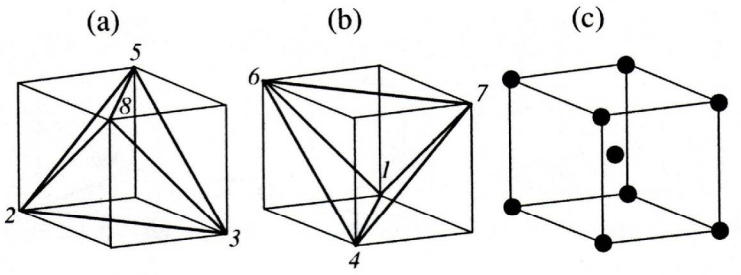

Fig. 3.

we invoke the definition (3.5) of a trilinear mapping to find

$$\begin{cases} \mathbf{w}_1^{\mathrm{T}}(\xi_1, \xi_2, \xi_3) \\ = (-(1-\xi_2)(1-\xi_3), (1-\xi_2)(1-\xi_3), -\xi_2(1-\xi_3), \xi_2(1-\xi_3), -(1-\xi_2)\xi_3, (1-\xi_2)\xi_3, -\xi_2\xi_3, \xi_2\xi_3), \\ \mathbf{w}_2^{\mathrm{T}}(\xi_1, \xi_2, \xi_3) \\ = (-(1-\xi_1)(1-\xi_3), -\xi_1(1-\xi_3), (1-\xi_1)(1-\xi_3), \xi_1(1-\xi_3), -(1-\xi_1)\xi_3, -\xi_1\xi_3, (1-\xi_1)\xi_3, \xi_1\xi_3), \\ \mathbf{w}_3^{\mathrm{T}}(\xi_1, \xi_2, \xi_3) \\ = (-(1-\xi_1)(1-\xi_2), -\xi_1(1-\xi_2), -(1-\xi_1)\xi_2, -\xi_1\xi_2, (1-\xi_1)(1-\xi_2), \xi_1(1-\xi_2), (1-\xi_1)\xi_2, \xi_1\xi_2). \end{cases} \tag{3.6}$$

To determine Q_i, it will suffice to choose a quadrature formula. In particular, the 8-point Gaussian quadrature satisfies the patch test and has a barrier property; however, this barrier does not guarantee that the trilinear mapping is invertible.

3.2.1. Compound elements. To construct a barrier that admits only well-shaped cells at $t = 0$ and does not require cumbersome calculations, let us consider the partitions of a hexahedron into auxiliary tetrahedra shown in Fig. 3.

Partitions of this kind are widely used in combination with the mixed finite element method [28]. The quasi-isometricity condition for a hexahedral cell is interpreted here as that for mappings of the ten tetrahedra shown in Fig. 3. It is clear that they include eight corner tetrahedra and two tetrahedra that should be associated with the cell center (see Fig. 3c). First of all, one should determine the type of mapping of the logical tetrahedron to the physical tetrahedron. Obviously, it should be a linear mapping. Denote by $\mathbf{v}_1, \ldots, \mathbf{v}_4$ and $\mathbf{l}_1, \ldots, \mathbf{l}_4$ the vertices of a tetrahedron τ in physical coordinates x_1, x_2, x_3 and of a tetrahedron T in logical coordinates ξ_1, ξ_2, ξ_3, respectively. We seek a covariant basis for the mapping $T \longrightarrow \tau$, which is easy to construct by using natural coordinates [24]. As a result, the following equation is obtained:

$$\begin{pmatrix} 1 \\ x_1 \\ x_2 \\ x_3 \end{pmatrix} = \begin{pmatrix} 1 & 1 & 1 & 1 \\ \mathbf{v}_1 & \mathbf{v}_2 & \mathbf{v}_3 & \mathbf{v}_4 \end{pmatrix} \begin{pmatrix} 1 & 1 & 1 & 1 \\ \mathbf{l}_1 & \mathbf{l}_2 & \mathbf{l}_3 & \mathbf{l}_4 \end{pmatrix}^{-1} \begin{pmatrix} 1 \\ \xi_1 \\ \xi_2 \\ \xi_3 \end{pmatrix}.$$

It is obvious that the basis vector components of the mappings corresponding to the corner tetrahedra are identical with those of the trilinear mapping at the respective vertices of the hexohedra. It remains to find the basis vectors for the "central" tetrahedra. First, consider the case illustrated by Fig. 3b. Here, $\mathbf{v}_1 = \mathbf{r}_1$, $\mathbf{v}_2 = \mathbf{r}_4$, $\mathbf{v}_3 = \mathbf{r}_6$, $\mathbf{v}_4 = \mathbf{r}_7$,

$$\mathbf{l}_1 = \begin{pmatrix} 0 \\ 0 \\ 0 \end{pmatrix}, \quad \mathbf{l}_2 = \begin{pmatrix} 1 \\ 1 \\ 0 \end{pmatrix}, \quad \mathbf{l}_3 = \begin{pmatrix} 1 \\ 0 \\ 1 \end{pmatrix}, \quad \mathbf{l}_4 = \begin{pmatrix} 0 \\ 1 \\ 1 \end{pmatrix}$$

and

$$\mathbf{g}_1 = \frac{1}{2}(\mathbf{v}_2 + \mathbf{v}_3 - \mathbf{v}_1 - \mathbf{v}_4), \quad \mathbf{g}_2 = \frac{1}{2}(\mathbf{v}_2 + \mathbf{v}_4 - \mathbf{v}_1 - \mathbf{v}_3), \quad \mathbf{g}_3 = \frac{1}{2}(\mathbf{v}_3 + \mathbf{v}_4 - \mathbf{v}_1 - \mathbf{v}_2).$$

The geometrical meaning of $\mathbf{g}_i$ is clear from Fig. 3b. The other "central" tetrahedron is analyzed in a similar manner. Summing up, we have the following results for the barrier approximation:

$$N_q = 10, \quad \sigma_1 = \ldots = \sigma_8 = 1/12, \quad \sigma_9 = \sigma_{10} = 1/6.$$

This choice of weighting factors ensures that the patch test conditions are fulfilled, as shown by O.V. Ushakova.

The matrices $Q_1, \ldots, Q_8$ corresponding to the cell vertices are written as

$$Q_{4k+2j+i} = \begin{pmatrix} \mathbf{w}_1^{\mathrm{T}}(i, j, k) \\ \mathbf{w}_2^{\mathrm{T}}(i, j, k) \\ \mathbf{w}_3^{\mathrm{T}}(i, j, k) \end{pmatrix}, \quad i, j, k \in \{0, 1\},$$

and the matrices Q_9 and Q_{10} corresponding to the "central" tetrahedra are

$$Q_9 = \frac{1}{2}\begin{pmatrix} 0 & 1 & -1 & 0 & -1 & 0 & 0 & 1 \\ 0 & -1 & 1 & 0 & -1 & 0 & 0 & 1 \\ 0 & -1 & -1 & 0 & 1 & 0 & 0 & 1 \end{pmatrix}, \quad Q_{10} = \frac{1}{2}\begin{pmatrix} -1 & 0 & 0 & 1 & 0 & 1 & -1 & 0 \\ -1 & 0 & 0 & 1 & 0 & -1 & 1 & 0 \\ -1 & 0 & 0 & -1 & 0 & 1 & 1 & 0 \end{pmatrix}.$$

These ten quadrature weighting factors and ten matrices Q_i completely characterize an approximation of the functional.

The barrier described here appears to be the simplest isotropic one. In principle, the approximation based only on five tetrahedra (as shown in Fig. 3a or 3b) also has a barrier property, but it is characterized by a substantial degree of anisotropy, which can undermine mesh quality.

It is clear that the approximation above can be used for smoothing unstructured tetrahedral grids.

3.2.2. Barrier admitting severely distorted cells. Nondegeneracy is a very stringent requirement for a local mapping. It naturally arises when the finite element method is applied, but is frequently redundant with regard to the finite volume method, which relies on the positivity condition for cell volume, the patch test condition, and some restrictions concerning admissible cell shape. In [27], it was shown that the weakest restriction of this kind is the positivity condition for the Jacobian of the trilinear mapping at the cell face centers, which is equivalent to the requirement that the cell be unfolded. However, the Jacobian may be negative at vertices and on edges; that is, a trilinear mapping proper becomes meaningless.

One example of such a barrier approximation, constructed in [27], is illustrated by Fig. 4, which shows two sets of basis vectors $\mathbf{g}_1$, $\mathbf{g}_2$, $\mathbf{g}_3$ of the 24 possible combinations. The remaining combinations are obtained through rotation in the logical coordinates. The matrices Q_1 and Q_2 corresponding to the bases shown in Fig. 4 are

$$Q_1 = \left(\mathbf{w}_1\left(\frac{1}{2}, 0, 0\right), \mathbf{w}_2\left(\frac{1}{2}, \frac{1}{2}, 0\right), \mathbf{w}_3\left(\frac{1}{2}, \frac{1}{2}, \frac{1}{2}\right)\right), \quad Q_2 = \left(\mathbf{w}_1\left(\frac{1}{2}, 0, 0\right), \mathbf{w}_2\left(\frac{1}{2}, \frac{1}{2}, \frac{1}{2}\right), \mathbf{w}_3\left(\frac{1}{2}, 0, \frac{1}{2}\right)\right).$$

Since the matrices $Q_3, \ldots, Q_{24}$ can be expressed in a similar form, they are not written out here. In this case, $\sigma_i = 1/24$.

3.2.3. Barrier that guarantees an invertible trilinear mapping. The covariant basis vectors of a trilinear mapping are defined as follows:

$$\mathbf{g}_i(\xi_i, \xi_k) = (1 - \xi_j)(1 - \xi_k)\mathbf{g}_i^{00} + \xi_j(1 - \xi_k)\mathbf{g}_i^{10} + (1 - \xi_j)\xi_k\mathbf{g}_i^{01} + \xi_j\xi_k\mathbf{g}_i^{11}, \tag{3.7}$$

where $\{i, j, k\}$ is a cyclic permutation of $\{1, 2\,3\}$, and

$$\mathbf{g}_1^{mn} = \mathbf{r}^{1mn} - \mathbf{r}^{0mn}, \quad \mathbf{g}_2^{mn} = \mathbf{r}^{m1n} - \mathbf{r}^{m0n}, \quad \mathbf{g}_3^{mn} = \mathbf{r}^{mn1} - \mathbf{r}^{mn0}, \quad m, n \in \{0, 1\}.$$

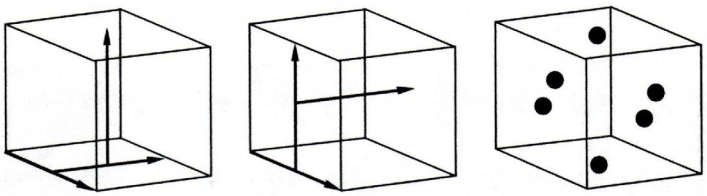

Fig. 4.

Using (3.7), one can write out the Jacobian of the trilinear mapping:

$$J = \sum_{i,j,k,l,m,n=0}^{1} \alpha_{k+m,i+n,j+l} \mathbf{g}_1^{ij} \cdot (\mathbf{g}_2^{kl} \times \mathbf{g}_3^{mn}), \tag{3.8}$$

where

$$\alpha_{pqr} = \xi_1^p (1-\xi_1)^{2-p} \xi_2^q (1-\xi_2)^{2-q} \xi_3^r (1-\xi_3)^{2-r}, \quad p, q, r \in \{0, 1, 2\}, \tag{3.9}$$

and α_{pqr} are strictly positive for the interior points of a trilinear cell. This means that, if

$$\mathbf{g}_1^{ij} \cdot (\mathbf{g}_2^{kl} \times \mathbf{g}_3^{mn}) > 0, \quad i, j, k, l, m, n \in \{0, 1\}, \tag{3.10}$$

then (3.8) implies that the Jacobian is positive at every interior point. Since at least one function α_{pqr} is positive on the boundary, J must be also positive on the boundary.

Thus, one is naturally led to an approximation based on $N_q = 64$, which ensures that every product in (3.10) is positive. The expressions for $Q_1, \ldots, Q_{64}$ are omitted here, because they are obvious, but cumbersome.

The total number of summands in (3.8) is 64. However, it is obvious that not all of them are independent. An analysis performed by Ushakova has shown that only $3^3 = 27$ different "basis" functions α_{pqr} are essentially different.

As a consequence, the expression in (3.8) can be represented as the sum of 27 basis functions whose coefficients are partial sums of the 64 triple products in (3.10). Thus, when the 27 coefficients are positive, the trilinear mapping is not degenerate. However, it is not clear yet how the 27 inequalities can be used to construct a barrier, and the formulation of simple sufficient conditions for invertibility remains an open problem to this day. One conjecture is that the barrier based on the ten tetrahedra shown in Fig. 3 lies inside the nondegeneracy barrier of the trilinear mapping. It is easy to construct an example of a positive J defined by (3.8) in the case when one of the ten tetrahedra has a zero volume, whereas counterexamples illustrating the converse situation have not yet been found.

3.2.4. Barriers for high-order accurate schemes. In [27], a harmonic functional was used as an example to demonstrate that the best method for constructing barriers for high-order accurate finite volume methods must be based on a hierarchical approach in which the restrictions due to a higher order of accuracy are added to the basic restrictions corresponding to low-order accurate methods.

This is inconsistent with the basic principles underlying the generation of "high-order" grids, which relies on biharmonic equations or high-order accurate schemes for elliptic generators. In particular, it was shown in [10] that, when the finite element method with biquadratic basis functions is applied to the generalized Dirichlet functional, the result is not unique, and spurious inadmissible grids are generated even for relatively simple domains. This effect appears to be due to the lack of barrier property in the corresponding discrete functional.

4. EXAMPLE OF THE BEHAVIOR OF THE FUNCTIONAL ON A GRID WITH A SINGLE INTERIOR NODE

One convenient method for visualizing the discrete functional (3.1) is based on an analysis of a low-dimensional problem in which the functional can be represented as a function of two variables. Such an analysis was presented in [11] for the 3×3 grid shown in Fig. 5a. It is also necessary to analyze the behavior of the functional in the three-dimensional case and to estimate the variation of the geometry of the feasible domain under contraction. For simplicity, the analysis is restricted to the case when $H = I$ and $G = I$.

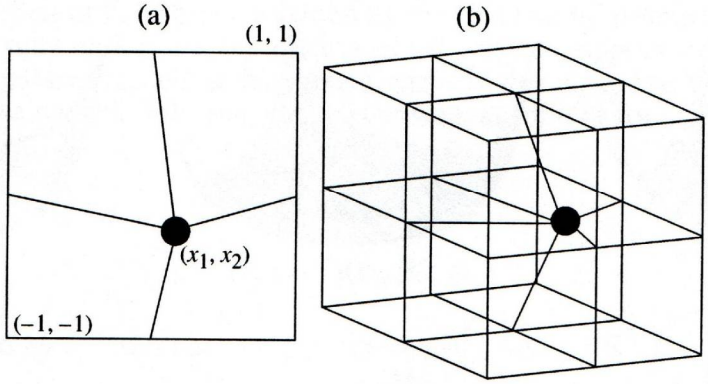

Fig. 5.

The three-dimensional case is obviously more difficult to analyze. Consider a $3 \times 3 \times 3$ structured grid in the cube $-1 \le x_i \le 1$ with 26 fixed nodes and one free node at $\mathbf{r} = (x_1, x_2, x_3)^{\mathrm{T}}$, where

$$\mathbf{r} = \mathbf{r}_0 + \mathbf{n}_1 y_1 + \mathbf{n}_2 y_2, \quad |\mathbf{n}_i| = 1, \quad \mathbf{n}_1^{\mathrm{T}} \mathbf{n}_2 = 0.$$

This configuration is shown in Fig. 5b, and the behavior of the function $u(y_1, y_2) = \mathcal{J}_\varepsilon^h(\mathbf{r}, t)$ is illustrated by Fig. 6. Here, approximation is based on composite elements with $N_q = 10$, $\mathbf{n}_1 = (1, 0, 0)^{\mathrm{T}}$, $\mathbf{n}_1 = (0, 1, 0)^{\mathrm{T}}$, and $\mathbf{r}_0 = 0$. Results obtained for a different choice of $\mathbf{r}$ or a two-dimensional configuration are qualitatively similar.

The top graphs in Fig. 6 correspond to $t = 0$, $t = 0.7$, and $t = 0.99$ (left to right), while $\varepsilon = 10^{-9}$ and $\omega_u = 0$. Here, the feasible domain is distinctly represented as a plateau by means of vertical scaling. All graphs are also scaled in the horizontal plane, because the feasible set behaves as a ball of radius $r \approx 0.8\sqrt{1-t}$ under contraction, which is confirmed by using sections defined by different $\mathbf{n}_1$ and $\mathbf{n}_2$. Similar behavior is observed in the two-dimensional case.

By construction, $u(y_1, y_2)$ is an infinitely smooth function. However, when ε is small, it involves narrow transition zones, which manifest themselves as discontinuities of the second kind in a numerical analysis. A semiempirical strategy for constructing a feasible solution without producing this effect was proposed in [11].

The bottom graphs in Fig. 6 represent similar cases with $\varepsilon = 0.0752$, $\varepsilon = 0.022$, and $\varepsilon = 0.0028$ (left to right), which corresponds to the continuation method in [11], in which ε is a function of the largest violation of the constraint: $\varepsilon \approx 0.2 q_{\min}$, where $q_{\min}$ is the negative value of $\det A - t\varphi(A)|_{q(c)}$ that has the largest absolute value. It is clear that there are no narrow transition zones in the bottom row.

Similar behavior is observed in the case of $\omega_u > 0$. As an example, Fig. 7 shows similar graphs obtained for $\omega_u = 0.8$. Those shown in the top row again correspond to $t = 0$, $t = 0.7$, and $t = 0.99$ (left to right), while $\varepsilon = 10^{-9}$. It is clear that the limit feasible set is a convex polyhedron with smoothed curved faces rather than a ball. Its characteristic diameter is also asymptotically proportional to $\sqrt{1-t}$.

The bottom graphs represent similar cases with $\varepsilon = 0.22$, $\varepsilon = 0.09934$, and $\varepsilon = 0.005$ (left to right), computed according to [11]. The regularizing effect is also obvious here.

5. ALGORITHM FOR MINIMIZATION AND CONTRACTION OF THE FEASIBLE SET

The two-parameter discrete minimization problem (3.1) was formulated in closed form in Section 3. As in [11], the first step in constructing a solution is such a scaling that the coordinates of nodes have values close to unity.

The iteration scheme is as follows:

$$\begin{gathered}\text{Take an initial approximation } t_0 = t_b \ge 0,\ \mathbf{R} = \mathbf{R}^0 \\ \text{if } q_{\min}(\mathbf{R}, t) < 0, \text{ then construct a feasible solution} \\ \textbf{for } k = 0, 1, 2, \ldots \\ \text{find an approximate solution to } \min_{\delta \mathbf{R}^k} \mathcal{J}_\varepsilon^h(\mathbf{R}^k + \delta\mathbf{R}^k, t_{k+1}), \text{ where } t_{k+1} = \beta(\mathbf{R}^k, t_k) \\ \mathbf{R}^{k+1} = \mathbf{R}^k + \delta\mathbf{R}^k.\end{gathered} \tag{5.1}$$

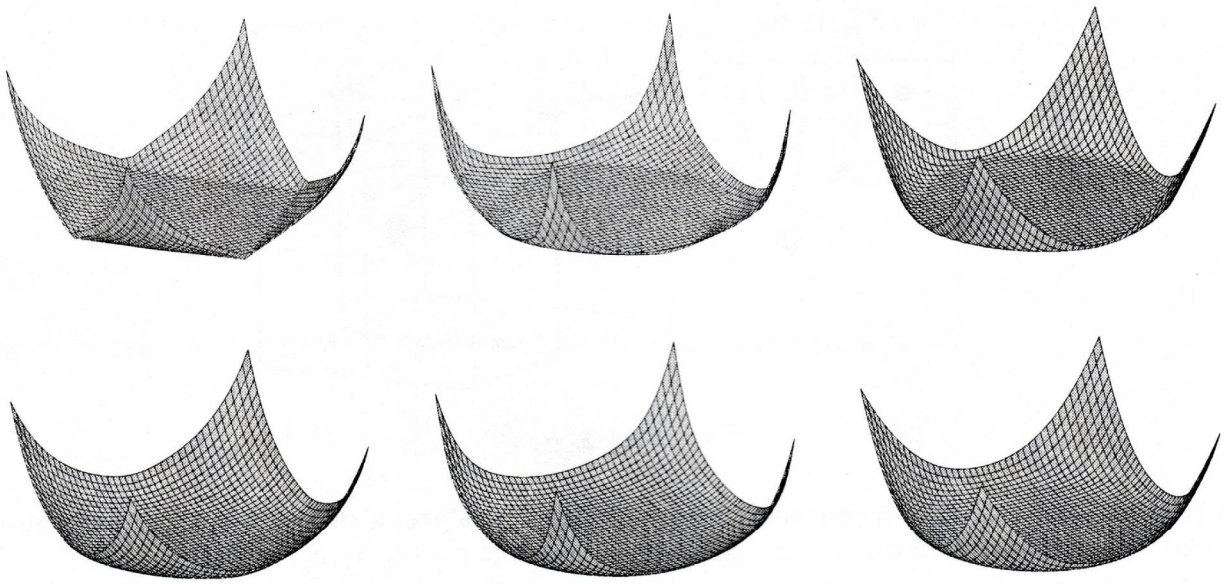

Fig. 6.

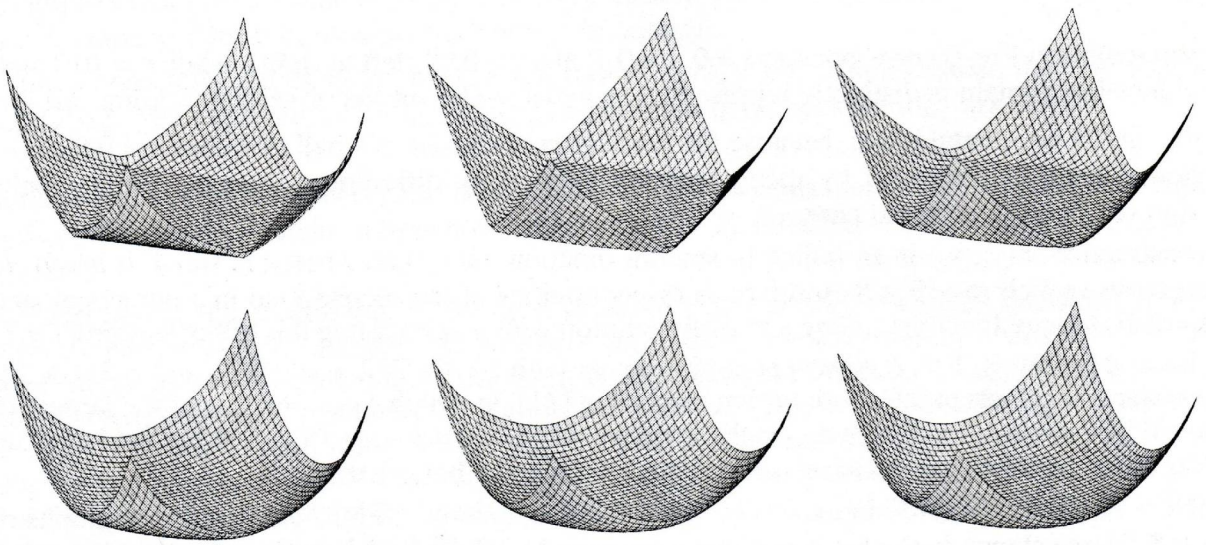

Fig. 7.

Here, $q_{\min}(\mathbf{R}, t)$ is the minimum of $q = \det A - t\varphi(A)$ over all quadrature points in all cells of $\mathbf{R}$, $\varepsilon_b = 10^{-9}$, and the function $\beta(\mathbf{R}, t)$ is defined as

$$\beta(\mathbf{R}, t) = \begin{cases} \max(t, (1-\delta)t_{\min}(\mathbf{R}) + \delta t_b), & q_{\min}(\mathbf{R}) > 0,\ t_{\min}(\mathbf{R}) > t, \\ t_{\min}(\mathbf{R}), & q_{\min}(\mathbf{R}, 0) > 0,\ q_{\min}(\mathbf{R}, t) \le 0, \\ t_b, & q_{\min}(\mathbf{R}, 0) < 0, \end{cases} \tag{5.2}$$

where

$$t_{\min}(R) = \min_{q(c)} \frac{\det A}{\varphi(A)}\bigg|_{q(c)},$$

and the parameter $\delta = 10^{-2}$ sets limits for contraction of the feasible set.

The complicated definition of $\beta(\mathbf{R}, t)$ is explained by the fact that minimization problem (5.1) is solved approximately [11]. This may undermine the quality of the iterative approximation, lead one beyond the limits of the feasible set, and even result in degenerate grids. In this case, one should again use an iterative algorithm for constructing a feasible solution, which is written as follows for an inadmissible initial approximation $\mathbf{R}^0$:

$$\textbf{for } k = 0, 1, 2, \ldots$$

$$\varepsilon_{k+1} = \gamma(\varepsilon_b, \mathbf{R}^k, t),$$

$$\text{find an approximate solution to } \min_{\delta\mathbf{R}^k} \mathcal{J}^h_{\varepsilon_{k+1}}(\mathbf{R}^k + \delta\mathbf{R}^k, t), \tag{5.3}$$

$$\mathbf{R}^{k+1} = \mathbf{R}^k + \delta\mathbf{R}^k,$$

$$\textbf{if } q_{\min}(\mathbf{R}^k, t) > 0, \text{ then } \varepsilon_{k+1} = \varepsilon_b, \text{ stop.}$$

The function γ is defined as follows [11]:

$$\gamma(\varepsilon, \mathbf{R}, t) = \sqrt{\varepsilon_b^2 + 0.04[\min(q_{\min}(\mathbf{R}, t), 0)]^2}. \tag{5.4}$$

An approximate solution to the minimization problem was obtained at each step by iterating once or twice the preconditioned gradient method based on the reduced Hessian of the functional $\mathcal{J}^h_{\varepsilon_k}$. It was found experimentally that feasible solutions are readily obtained for $\mathcal{F}^h(0)$ but are very difficult to construct for large values of t. For this reason, the value $t_b = 0$ was used, and the function β was chosen so as to keep the current approximation admissible while expanding or contracting the feasible set, while the continuation method (5.3) was applied only for correcting degenerate grids. It is clear that the algorithm described here is a heuristic one. An algorithm that admits a substantiation can be constructed if the minimization problem can be solved exactly for a fixed t. However, such an algorithm would obviously be of no practical value. Therefore, approximate minimization algorithms must be validated, and their convergence must be proved. Practical application of the algorithm described here demonstrated that it is reliable and effective in contracting the feasible set.

6. NUMERICAL EXPERIMENTS

6.1. Domain with Nonconvex Corners

In the first series of numerical experiments, grid generation was analyzed for the domain shown in Fig. 8, where two unit squares are shifted by the vector $(3/10, -3/10)^T$ relative to each other. All quasi-isometric grids were generated for $\omega_n = 0.8$. Let us show that the condition number of a quasi-isometric grid is a slowly decreasing function of the number of cells approaching a plateau, whereas the condition number of a harmonic grid increases faster than $O(N_v^{1/2})$; i.e., harmonic grids are not quasi-isometric when $G = I$:

Grid	11×21	21×41	41×81	81×161
Γ/γ	10.5	8.53	7.93	8.06
$\Gamma/\gamma\|_{\text{harmonic}}$	58.9	118.5	320.8	743.7

Examples of grids generated for this geometry are shown in Fig. 8 to demonstrate why the harmonic grid (a) is so poorly conditioned. On the other hand, it is smoother in the greater part of the domain, and the greater condition number should be attributed to effects localized at the boundary.

In this problem, multiple solutions could not be obtained. A similar, but more stiff, problem was considered in [11], where the nonuniqueness of the solution was demonstrated for the barrier method. Numerical experiments showed that contraction of the feasible set is not sufficient for dealing with the problem. Moreover, finding the best solution is not worthwhile: all grids corresponding to stationary points are close to each other, and global optimization would not be cost-effective.

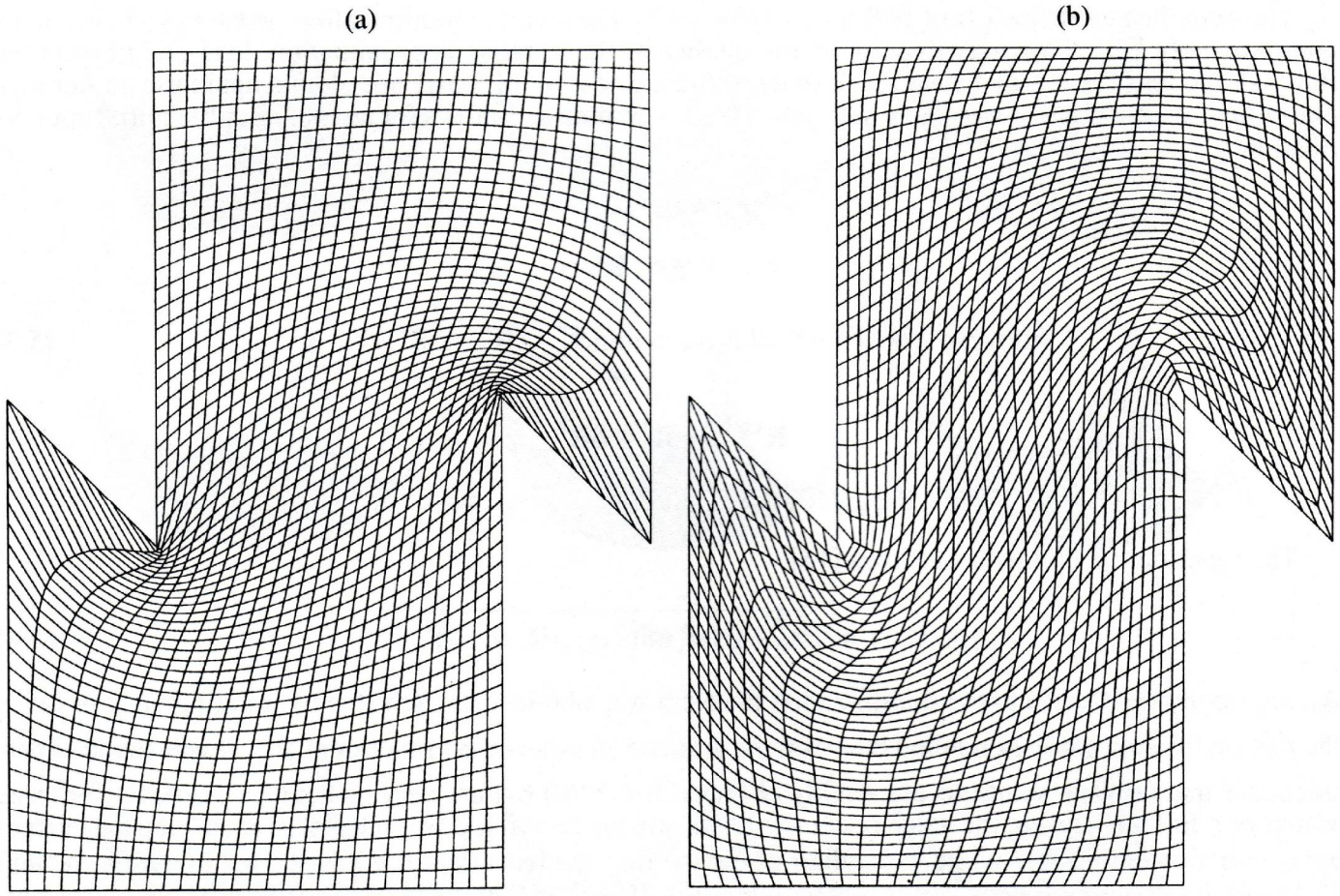

Fig. 8.

6.2. Condensation toward a Domain Boundary

In the second series of problems, the same domain was analyzed with the use of a control metric H^TH, where $H = H(\xi_1)$. The matrix H was obtained through difference differentiation of the auxiliary mapping

$$f(\xi_1) = \xi_1 - \frac{1}{2\pi}(n_1 - 1)b\sin\frac{2\pi(\xi_1 - 1)}{n_1 - 1}, \quad 1 \le \xi_1 \le n_1, \tag{6.1}$$

which corresponds to a cell with bottom left vertex with indices i_1 and i_2,

$$h_{11} = f(i_1 + 1) - f(i_1), \quad h_{22} = 1, \quad h_{12} = h_{21} = 0.$$

This normalization was used because each cell is a unit square in the logical coordinates. The grid points lying on the upper and lower horizontal boundaries were arranged according to (6.1):

$$x_1(\xi_1) = x_1|_{\text{corner}} + [f(\xi_1) - 1]/(n_1 - 1).$$

The parameter b was set equal to 0.95, which means quite a high degree of condensation of lines $\xi_1 = \text{const}$ toward lateral boundaries.

Examples of harmonic and quasi-isometric grids are presented in Fig. 9. Here, the disparity between the two approaches is even more pronounced:

Grid	11×11	21×21	41×41	81×81
Γ/γ	19.9	7.9	7.34	7.44
$\Gamma/\gamma\|_{\text{harmonic}}$	261	10^3	2.71×10^3	5.7×10^3

It is clearly seen that, if the quasi-isometric grid is sufficiently fine, then its condition number is close to a constant that is virtually the same both with and without condensation. This constant appears to be a characteristic of the domain. However, the condition number of a harmonic grid with the metric H^TH rapidly increases with the degree of condensation.

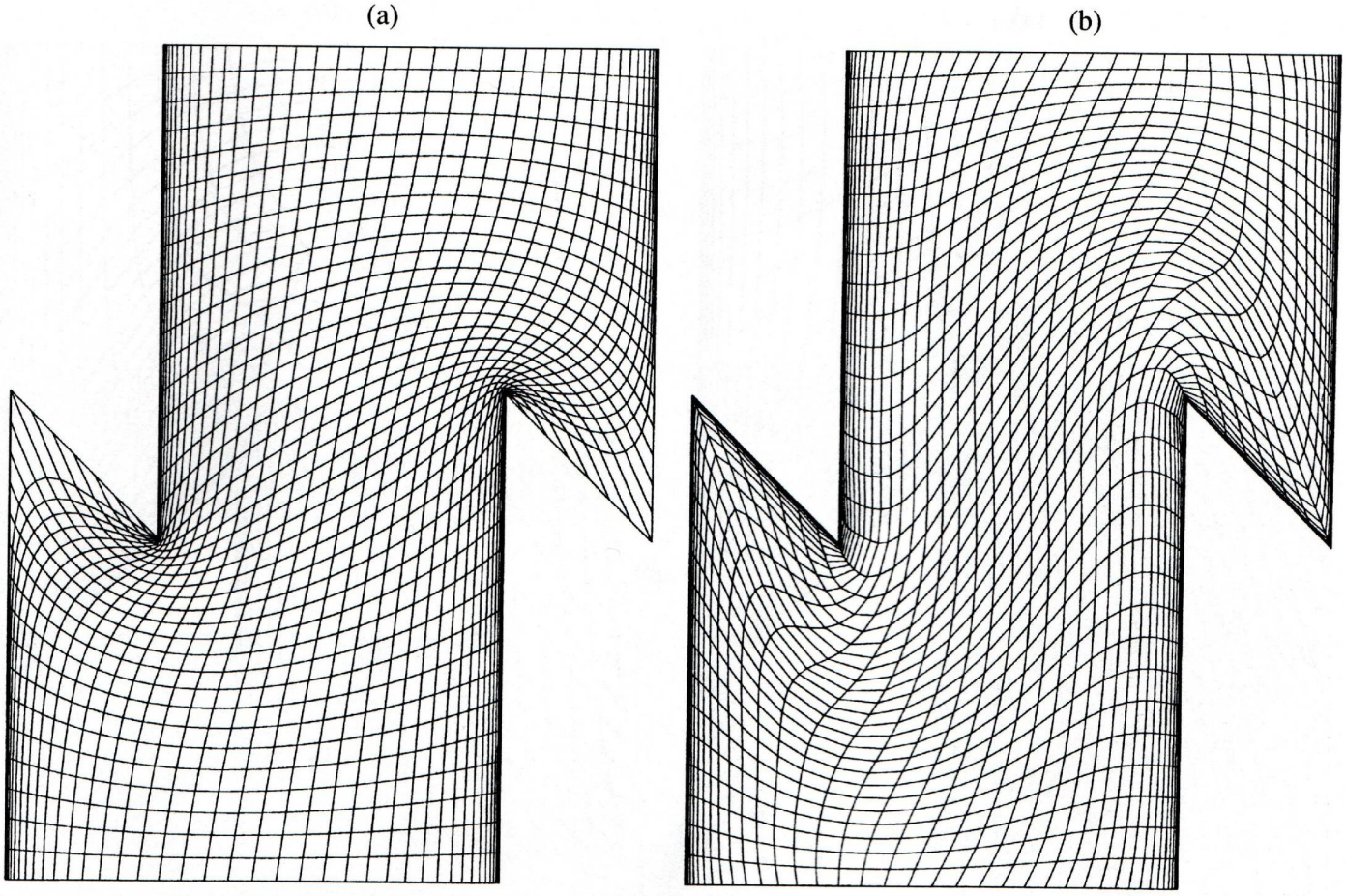

Fig. 9.

6.3. Orthogonality at the Domain Boundary

The quasi-isometric grids generated for a domain with corners in the preceding example were characterized by a low condition number but were not orthogonal at the domain boundary. To ensure the orthogonality, functional (2.13) can be used with

$$\psi(H) = \bar{h}/\det H, \quad \bar{h} = \frac{1}{N_c}\sum_{c=1}^{N_c}\int_{\mathcal{D}_c}\det H\, d\xi.$$

Figure 10a shows a magnified grid fragment characterized by the same size and definition of the metric H (see (6.1)) as that shown in Fig. 9a but obtained by using functional (2.13) with $t = 0$ and $\omega_u = 0$, i.e., without using any compressibility-controlling term and without contracting the feasible set. This grid is characterized by the condition number 21.3. Figure 10b shows a grid fragment generated by using (2.13) with $\omega_u = 0.8$ and by contracting the feasible set. Here, the condition number is 16. It may seem that the two grids are just slightly different. However, the quasi-isometric grid is characterized by a cell size along the normal to the boundary is close to that determined by (6.1), whereas the corresponding cell size in the "harmonic" grid is greater by a factor of 2 to 3. It should be noted that a simple modification of the harmonic functional through the introduction of the factor $\psi(H)$ substantially improves the quality of condensed grids and sometimes makes it possible to avoid contracting the feasible set.

6.4. Drop-Shaped Domain

The domain with a drop-shaped portion of its boundary is a standard test for grid generation methods, since domains of this shape are frequently encountered in various problems of hydrodynamic instability of fluid interfaces. It is well known that the harmonic method with a constant metric leads to poor results as applied to this geometry, so that the problem was solved by using various additional devices, such as

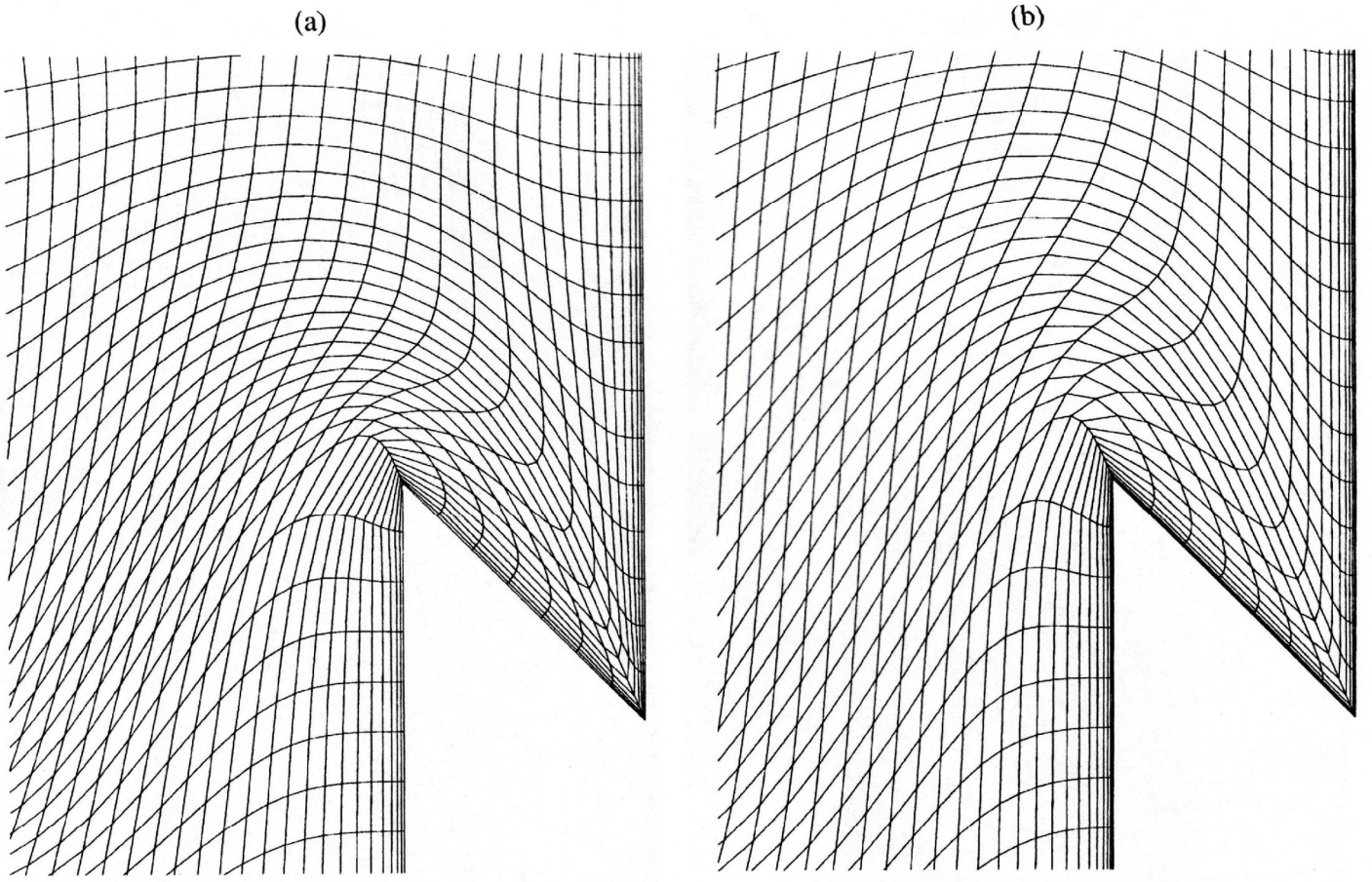

Fig. 10.

uniformity conditions imposed via introducing Lagrange multipliers, auxiliary one-dimensional mappings, etc.

The harmonic and quasi-isometric grids shown in Fig. 11 are characterized by the condition numbers 51.2 and 15.4, respectively. The quasi-isometric grid was generated for $\omega_u = 0.95$ even though both grid and condition number vary little when ω_u is varied between 0.8 and 0.95. Since the boundary is smooth in this example, one can use ω_u close to unity. However, this cannot be done in the general case, because the Euler–Lagrange equations for functional (2.11) can change type when $\omega_u \geq 1$. Grids generated for domains with nonsmooth boundaries are also nonsmooth. On average, the optimal parameter value is $\omega_u = 0.8$.

6.5. Example of an Adaptive Grid

Comparison between different adaptation strategies is a very difficult task, primarily because it depends on a specific application. For this reason, the examples presented here demonstrate only a qualitative difference between grids. Consider grid generation in the unit square $0 < x_i < 1$ with a prescribed metric $G = G(\mathbf{r})$, which is chosen so that the grid condenses in zones of steep gradient of a certain function $u = u(x_1, x_2)$. For the harmonic method, the metric was defined so that the grid on the surface of the graph of $u(x_1, x_2)$ was as close to a uniform one as possible. According to [5, 7], this condition leads to

$$G = \{g_{ij}\}, \quad g_{11} = 1 + \left(\frac{\partial u}{\partial x_1}\right)^2, \quad g_{22} = 1 + \left(\frac{\partial u}{\partial x_2}\right)^2, \quad g_{12} = \frac{\partial u}{\partial x_1}\frac{\partial u}{\partial x_2}, \tag{6.2}$$

while a simplified metric was used to generate a quasi-isometric grid:

$$G = (1 + |\nabla u|^2)^{1/2} I. \tag{6.3}$$

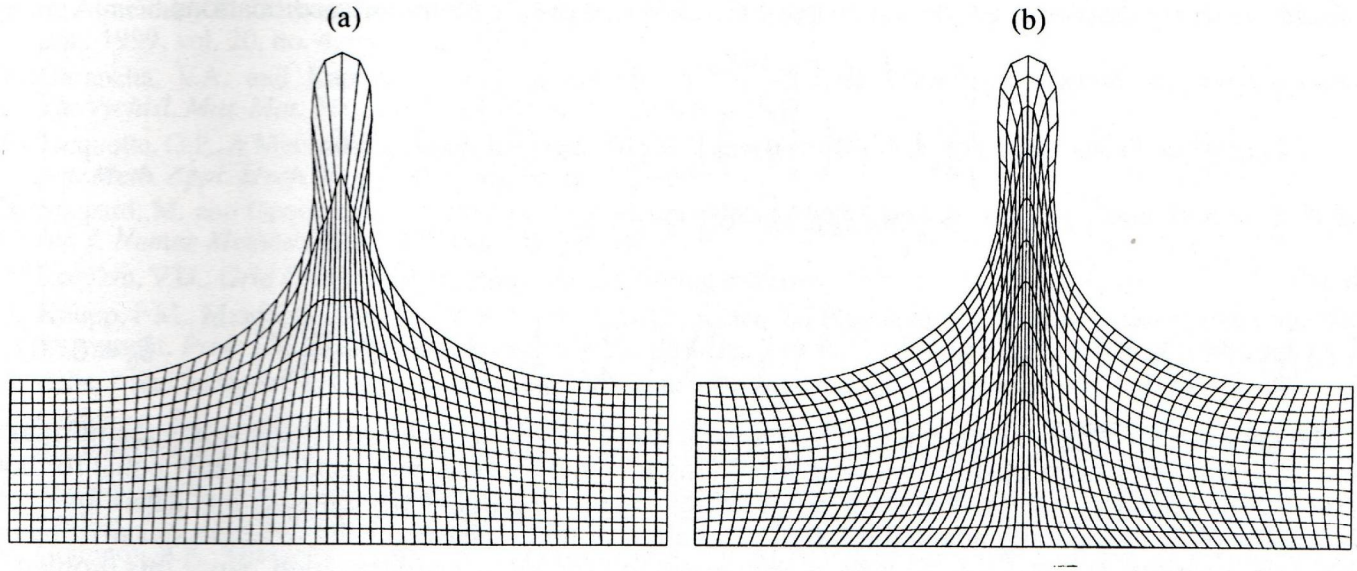

Fig. 11.

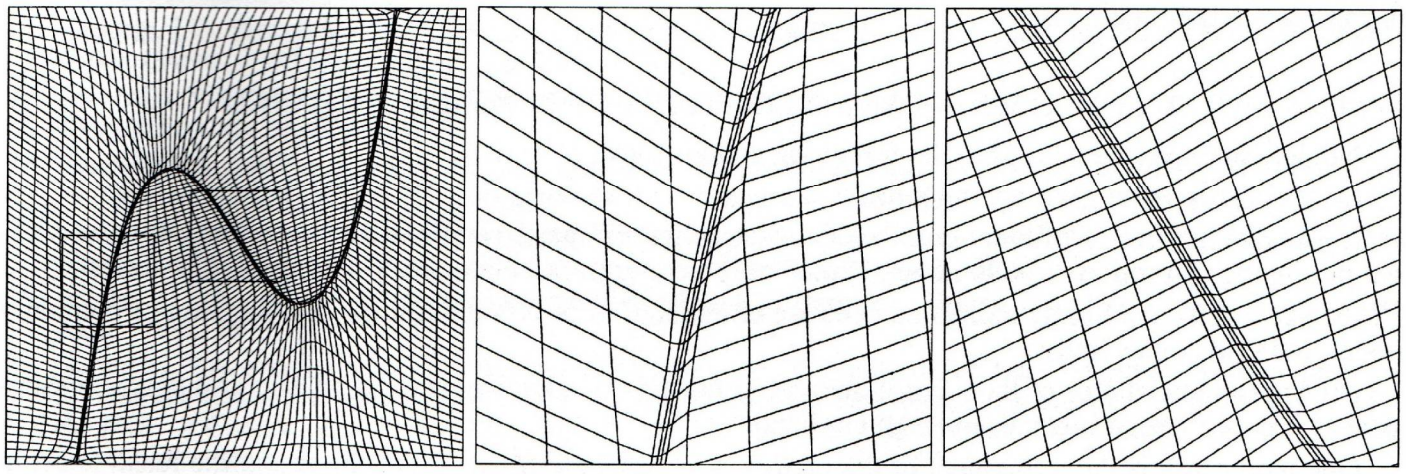

Fig. 12.

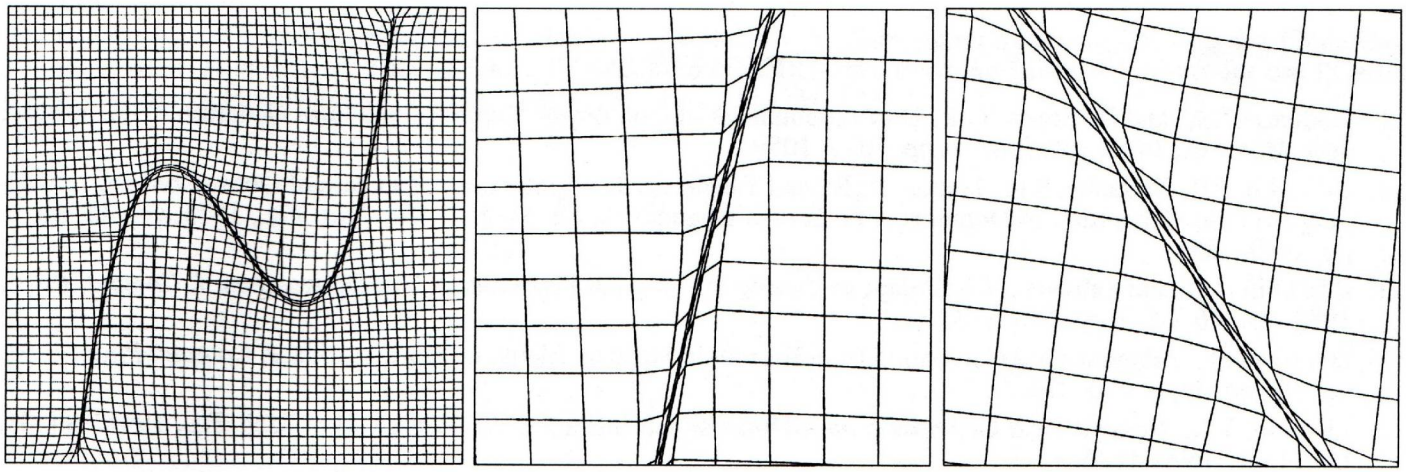

Fig. 13.

In the case of functional (2.11), both metrics are suitable, whereas only (6.2) can be used in a harmonic functional. For this reason, examples with different metrics are compared here, which makes the comparison biased towards the harmonic method. For example, it is clear that grids generated on surfaces should be compared with metrics given by (6.2). Figures 12 and 13 show examples of quasi-isometric and harmonic

grids, respectively. As a test, a function proposed in [25] was used with minor modifications

$$u = \begin{cases} c, & \text{if } x_2 \geq y_0 + \delta, \\ \dfrac{c}{2}\left(1 + \sin\left(\pi\left(q - \dfrac{1}{2}\right)\right)\right), & \text{if } y_0 - \delta \leq x_2 \leq y_0 + \delta, \\ 0, & \text{if } x_2 \leq y_0 - \delta, \end{cases}$$

where

$$q = \frac{1}{2\delta}(x_2 - y_0 + \delta), \quad y_0(x_1) = 25\left(x_1 - \frac{1}{2}\right)\left(x_1 - \frac{3}{4}\right)\left(x_1 - \frac{1}{4}\right) + \frac{1}{2}, \quad \delta = \delta_0\left[1 + \left(\frac{\partial y_0}{\partial x_1}\right)^2\right]^{1/2}, \quad \delta_0 = 0.002.$$

The parameter c differed between the two cases. It was adjusted so that the cell size along the normal to the narrow transition zone of steep gradient simulating a boundary layer was approximately equal for both methods. The boundary points were fixed in both cases. Figures 12 and 13 demonstrate that a harmonic grid with metric (6.2) is generally adapted through generation of highly skewed cells, whereas quasi-isometric grids with metric (6.3) turn out to be almost orthogonal in the zones of condensation. Since this problem is quite restrictive, neighboring cells are characterized by an abrupt change in size. This defect can be corrected by choosing a function u with a different local behavior in the transition zone. However, this situation is common to both methods.

7. CONCLUSIONS AND DIRECTIONS OF FURTHER RESEARCH

Numerical experiments lead to the following conclusions:

(a) Quasi-isometric grids are smooth;

(b) As distinct from harmonic grids with constant metrics, quasi-isometric grids can be generated without producing disproportionately large or small cells near convex or concave portions of the boundary;

(c) Skew cells and highly elongated cells are eliminated, if possible, for a specific location of boundary nodes and grid connectivity;

(d) Appropriate choice of the control metric $G(\mathbf{r})$ makes an adaptive quasi-isometric grid nearly orthogonal as it is condensed in zones of steep gradients.

One major task is the refinement of the method used for minimizing and contracting the feasible set in the case of $G = G(\mathbf{r})$, because exact calculation of the gradient and Hessian of a discrete functional is difficult in this case. Conditions that guarantee a unique solution remain to be found yet. Certainly, the most important task is the analysis of the performance of the method in the three-dimensional case.

REFERENCES

1. Godunov, S.K. and Prokopov, G.P., On Computations of Conformal Mappings and Grid Generation, *Zh. Vychisl. Mat. Mat. Fiz.*, 1967, vol. 7, no. 5, pp. 1031–1059.
2. Belinskii, P.P., Godunov, S.K., Ivanov, Yu.B., and Yanenko, I.K., Application of a Class of Quasi-Conformal Mappings to Grid Generation in Domains with Curved Boundaries, *Zh. Vychisl. Mat. Mat. Fiz.*, 1975, vol. 15, no. 6, pp. 1499–1511.
3. Brackbill, J.U. and Saltzman, J.S., Adaptive Zoning for Singular Problems in Two Dimensions, *J. Comput. Phys.*, 1982, vol. 46, no. 3, pp. 342–368.
4. Dvinsky A.S., Adaptive Grid Generation from Harmonic Maps on Riemannian Manifolds, *J. Comput. Phys.*, 1991, vol. 95, no. 3, pp. 450–476.
5. Liseikin, V.D., Regular Grid Generation on n-Dimensional Surfaces, *Zh. Vychisl. Mat. Mat. Fiz.*, 1991, vol. 31, no. 11, pp. 1670–1683.
6. Ivanenko, S.A. and Charakhch'yan, A.A., Curvilinear Convex Quadrilateral Grids, *Zh. Vychisl. Mat. Mat. Fiz.*, 1988, vol. 28, no. 4, pp. 503–514.
7. Charakch'yan, A.A. and Ivanenko, S.A., A Variational Form of the Winslow Grid Generator, *J. Comput. Phys.*, 1997, vol. 136, pp. 385–398.
8. Antman, S.S., Regular and Singular Problems for Large Elastic Deformations of Tubes, Wedges, and Cylinders, *Arch. Ration. Mech. Analys.*, 1982, vol. 83, pp. 1–52.
9. Ciarlet, P. G., *Mathematical Elasticity, Vol. 1 (Studies in Mathematics and Its Applications, vol. 20)*, New York: Elsevier, 1988.

10. de Almeida, V.F., Domain Deformation Mapping: Application to Variational Mesh Generation, *SIAM J. Sci. Comput.*, 1999, vol. 20, no. 4, pp. 1252–1275.
11. Garanzha, V.A. and Kaporin, I.E., Regularization of the Barrier Variational Method of Grid Generation, *Zh. Vychisl. Mat. Mat. Fiz.*, 1999, vol. 39, no. 9, pp. 1489–1503.
12. Jacquotte, O.P., A Mechanical Model for a New Grid Generation Method in Computational Fluid Dynamics, *Comput. Meth. Appl. Mech. Eng.*, 1988, vol. 66, pp. 323–338.
13. Shepard, M. and Georges, M., Automatic Three-Dimensional Mesh Generation by the Finite Octree Technique, *Int. J. Numer. Methods Eng.*, 1991, vol. 32, pp. 709–749.
14. Liseikin, V.D., *Grid Generation Methods*, Berlin: Springer-Verlag, 1999.
15. Knupp, P.M., Matrix Norms & the Condition Number: A General Framework to Improve Mesh Quality via Node-Movement, *Proc. 8th Int. Meshing Roundtable, South Lake, Tahoe, California, October 10–13,* 1999, pp. 13–22.
16. Eells, J. and Sampson, J., Harmonic Mappings of Riemannian Manifolds, *Am. J. Math.*, 1964, vol. 86, pp. 109–160.
17. Godunov, S.K., Zabrodin, A.V., Ivanov, M.Ya., *et al.*, *Chislennoe reshenie mnogomernykh zadach gazovoi dinamiki* (Numerical Solution of Multidimensional Problems in Gas Dynamics), Moscow: Nauka, 1976.
18. Marshall, A.W. and Olkin, I.N., *Inequalities: The Theory of Majorizations and Its Applications,* New York: Academic, 1979. Translated under the title *Neravenstva: teoriya mazhorizatsii i ee prilozheniya,* Moscow: Mir, 1983.
19. Godunov, S.K., Gordienko, V.M., and Chumakov, G.A., Quasi-Isometric Parameterization of a Curvilinear Quadrangle and a Metric of Constant Curvature, *Sib. Adv. Math.*, 1995, vol. 5, no. 2, pp. 1–20.
20. Evtushenko, Yu.G. and Zhadan, V.G., Exact Auxiliary Functions in Optimization Problems, *Zh. Vychisl. Mat. Mat. Fiz.*, 1990, vol. 30, no. 1, pp. 43–57.
21. Kaporin, I.E., Preconditioned Conjugate Gradient Method for Difference Counterparts of Differential Problems, *Differ. Uravn.*, 1990, vol. 26, no. 7, pp. 1225–1236.
22. Garanzha, V.A., Barrier Variational Generation of Quasi-Isometric Grids, *Research Report No. 0007*, Nijmegen: Katholieke Univ. Nijmegen, 2000.
23. Riemslagh, K. and Vierendeels, J., Grid Generation for Complex Shaped Moving Domains, in *Proc. of the 5th Int. Conf. on Numerical Grid Generation in Computational Field Simulation*, Starkville, Miss.: ERC, 1996, pp. 569–578.
24. Strang, G. and Fix, G.J., *An Analysis of the Finite Element Method*, Englewood Cliffs, N.J.: Prentice-hall, 1973. Translated under the title *Teoriya metoda konechnykh elementov*, Moscow: Mir, 1977.
25. Ivanenko, S.A., *Adaptivno-garmonicheskie setki* (Adaptive Harmonic Grids), Moscow: Vychisl. Tsentr Ross. Akad. Nauk, 1997.
26. Garanzha, V.A. and Kaporin, I.E., Variational Generation of Grids around Arbitrary Trajectory Wells in Reservoir Simulation, *Numerical Grid Generation in Computational Field Simulations: Proc. of the 6th Int. Conf., Held at the Univ. of Greenwich, July 6–July 9, 1998*, Cross, M. *et al.*, Eds., Mississippi State (Miss.): NSF Engineering Research Center for Computational Field Simulation, 1998, pp. 1001–1010.
27. Garanzha, V.A., Kaporin, I.E., and Konshin, V.N., Reliable Flow Solver Based on the High Order Control Volume Padé-type Differences, *Sixteenth International Conference on Numerical Methods in Fluid Dynamics: Proceedings of the Conference Held in Arcachon, France, 6–10 July, 1998,* Bruneau, C.-H., Ed., Berlin: Springer-Verlag, 1998, pp. 278–283.
28. Ewing, R.E., Kuznetsov, Y.A., Lazarov, R.D., and Maliassov, S., Substructuring Preconditioning for Finite Element Approximations of Second Order Elliptic Problems. I. Nonconforming Linear Elements for the Poisson Equation in a Parallelepiped, *ISC Res. Rept.*, ISC-94-02-MATH, 1994.